UV-inducible cellular aggregation of the hyperthermophilic archaeon Sulfolobus solfataricus is mediated by pili formation

Froels, Sabrina; Ajon, Malgorzata; Wagner, Michaela; Teichmann, Daniela; Zolghadr, Behnam; Folea, Mihaela; Boekema, Egbert J.; Driessen, Arnold J. M.; Schleper, Christa; Albers, Sonja-Verena

Published in:
Molecular Microbiology

DOI:
10.1111/j.1365-2958.2008.06459.x

Publication date:
2008

Molecular Microbiology (2008) 70(4), 938–952 ■
doi:10.1111/j.1365-2958.2008.06459.x
First published online 9 October 2008

UV-inducible cellular aggregation of the hyperthermophilic archaeon *Sulfolobus solfataricus* is mediated by pili formation

Sabrina Fröls,[1,2] Malgorzata Ajon,[3] Michaela Wagner,[3] Daniela Teichmann,[1] Behnam Zolghadr,[3] Mihaela Folea,[4] Egbert J. Boekema,[4] Arnold J. M. Driessen,[3] Christa Schleper[1,2]* and Sonja-Verena Albers[3]

[1]*Department of Genetics in Ecology, Vienna Ecology Center, University of Vienna, Althanstrasse 14, 1090 Vienna, Austria.*

[2]*Center for Geobiology, Department of Biology, University of Bergen, Realfagbygget, Allegaten 41, N-5007 Bergen.*

[3]*Department of Microbiology, Groningen Biomolecular Sciences and Biotechnology Institute and the Zernike Institute for Advanced Materials, University of Groningen, Kerklaan 30, 9751 NN Haren, the Netherlands.*

[4]*Department of Biophysical Chemistry, Groningen Biomolecular Sciences and Biotechnology Institute, University of Groningen, Nijenborgh 4, 9747 AG Groningen, the Netherlands.*

Summary

The hyperthermophilic archaeon *Sulfolobus solfataricus* has been shown to exhibit a complex transcriptional response to UV irradiation involving 55 genes. Among the strongest UV-induced genes was a putative pili biogenesis operon encoding a potential secretion ATPase, two pre-pilins, a putative transmembrane protein and a protein of unknown function. Electron microscopy and image reconstruction of UV-treated cells showed straight pili with 10 nm in diameter, variable in length, not bundled or polarized and composed of three evenly spaced helices, thereby clearly being distinguishable from archaeal flagella. A deletion mutant of SSO0120, the central type II/IV secretion ATPase, did not produce pili. It could be complemented by reintroducing the gene on a plasmid vector. We have named the operon *ups* operon for UV-inducible pili operon of *Sulfolobus*. Overexpression of the pre-pilins, Ups-A/B (SSO0117/0118) in *Sulfolobus* resulted in production of extremely long filaments. Pronounced cellular aggregation was observed and quantified upon UV treatment. This aggregation was a UV-dose-dependent, dynamic process, not inducible by other physical stressors (such as pH or temperature shift) but stimulated by chemically induced double-strand breaks in DNA. We hypothesize that pili formation and subsequent cellular aggregation enhance DNA transfer among *Sulfolobus* cells to provide increased repair of damaged DNA via homologous recombination.

Accepted 11 September, 2008. *For correspondence. E-mail christa.schleper@univie.ac.at; Tel. (+43) 14277 57800; Fax (+43) 14277 9578.

Introduction

The ability of *Bacteria* and *Archaea* to form multicellular structures is observed in a variety of biological systems. This fascinating phenomenon of a collective behaviour can be manifested in the formation of biofilms from mixed microbial mats, cellular aggregates or microcolonies. Multicellular structures represent an essential strategy for adaptation to changing environmental conditions or even survival (Shapiro, 1998; Davey and O'Toole, 2000; Battin *et al.*, 2007). Cells organized in biofilm-like structures show a higher resistance to toxic compounds, as for example antimicrobials (Patel, 2005) or to physical stress, like shifts in temperature or pH, or exposure to UV light (Ojanen-Reuhs *et al.*, 1997; Roine *et al.*, 1998; Elasri and Miller, 1999; Martinez and Casadevall, 2007). In addition, microorganisms benefit from the attachment on substrates like, e.g. suspended particles, which provides a higher nutrient availability (Davey and O'Toole, 2000). Also genetic transfer, i.e. DNA exchange via conjugation, plays an important role in biofilms to disseminate specific genes of metabolic pathways (Gasson and Davies, 1980; Molin and Tolker-Nielsen, 2003). The rate of conjugative DNA exchange in biofilm structures is enhanced and conjugative pili stabilize the biofilm structure (Gasson and Davies, 1980; Ghigo, 2001; Molin and Tolker-Nielsen, 2003; Reisner *et al.*, 2006).

Cellular aggregation is mainly reported for organisms of the domain *Bacteria*, while comparably few but quite

diverse examples have been found in the domain of the *Archaea*. In anoxic sediments of the ocean anaerobic methane-oxidizing archaea form synergistic communities with sulphate-reducing bacteria in the form of structured consortia (Boetius *et al*., 2000). An unusual microbial community organized in string-of-pearls was found in cold sulphurous water. It is formed by the euryarchaeon SM1 that grows in close association with the bacterium *Thiothrix* sp. and forms complex and unusual cellular appendages (Moissl *et al*., 2003; 2005). Single-strain cultures of the hyperthermophilic euryarchaeote *Archaeoglobus fulgidus* form a protein-, metal- and polysaccharide-containing heterogeneous biofilm, which is inducible by various environmental stressors (LaPaglia and Hartzell, 1997). *Pyrococcus furiosus* can form surface attached microcolony structures mediated by multifunctional flagella, which can also form cable-like structures to mediate cell–cell contacts (Näther *et al*., 2006; Schopf *et al*., 2008).

Beside adherent multicellular structures that are found attached to diverse surfaces, non-adherent floating multicellular structures are also described for archaea. *Methanosarcina mazei*, for example, forms aggregates during exponential growth (Mayerhofer *et al*., 1992) and halophilic archaea do so in the presence of divalent cations (Kawakami *et al*., 2005; 2007). For the halophilic euryarchaeote *Halobacterium volcanii* and the hyperthermophilic crenarchaeote *Sulfolobus* sp. cellular aggregation was observed in context with conjugative DNA transfer (Rosenshine *et al*., 1989; Schleper *et al*., 1995).

Characteristic for all types of cellular aggregation is the attachment between single cells, mostly mediated or stabilized by exopolysaccharides (EPS) and/or proteins as was shown for many bacterial systems (Davey and O'Toole, 2000; Klemm *et al*., 2004; Kawakami *et al*., 2007). Some microorganisms like *Xanthomonas* and *Pseudomonas* use type IV pili to initiate or mediate the cellular aggregation (Ojanen-Reuhs *et al*., 1997; Bhattacharjee *et al*., 2001). A *Pseudomonas aeruginosa* mutant defective in the type IV pilus biogenesis was unable to attach on surfaces and form microcolonies (O'Toole and Kolter, 1998; O'Toole *et al*., 2000).

The type IV pili biogenesis pathways of bacteria are not only closely related to the type II protein secretion systems (Sauvonnet *et al*., 2000; Köhler *et al*., 2004), but also to the archaeal flagella systems. This was shown by bioinformatic and biochemical analyses (Faguy *et al*., 1994; Bardy and Jarrell, 2002; Peabody *et al*., 2003). In addition, it has been shown that the flagella of *Halobacterium salinarum* and *Sulfolobus shibatae* are in symmetry and structure more closely related to the bacterial type IV pili than to bacterial flagella (Cohen-Krausz and Trachtenberg, 2002; 2008). The core components of the bacterial and archaeal systems are: (i) a type II/IV secretion system ATPase, (ii) a multispanning transmembrane protein, and (iii) the pre-pilin-like proteins with a characteristic N-terminal signal sequence (termed class III signal peptides) that form the structure of the pilus (Peabody *et al*., 2003). In the genome of the crenarchaeote *Sulfolobus solfataricus* three putative type IV pili loci were identified (Albers and Driessen, 2005). The operon SSO2316 (named after the central ATPase) codes for the flagellum of *S. solfataricus* (Szabó *et al*., 2007a). The operon SSO2680 encodes a recently described bindosome assembly system (Bas) needed for the functional surface localization of sugar-binding proteins (Zolghadr *et al*., 2007). The biological function of the third operon SSO0120, spanning ORFs *sso0117* through *sso0121*, was unclear. Using whole-genome microarray studies to analyse the UV response of *S. solfataricus* we observed that the genes *sso0117* to *sso0121* were among the most highly induced genes using a UV dose of 75 J m^{-2} at 254 nm (Fröls *et al*., 2007). A strong upregulation of the operon was also observed by an independent study of White and co-workers using a higher UV dose of 200 J m^{-2}, with *S. solfataricus* and *S. acidocaldarius* (Dorazi *et al*., 2007; Götz *et al*., 2007). In parallel to the strong transcriptional UV response we observed a massive aggregation of the cells, which disappeared after regeneration (Fröls *et al*., 2007).

In this study we demonstrate that extracellular pili-like structures, thinner than flagella, are formed upon UV light treatment. They are encoded by the UV-inducible (type IV-like) pili operon, as shown by targeted gene knockouts. Furthermore, we show that these pili structures are essential for the UV-dependent auto-aggregation of *S. solfataricus* cells and that this phenomenon is driven by double-strand breaks (DSB) in the DNA, but not by other stressors, such as pH or temperature shifts.

Results

UV-inducible expression of the sso0117–sso0121 *gene cluster*

The induction of the genes *sso0118* and *sso0117* occurred as one of the strongest and fastest transcriptional reactions detected in an earlier genome-wide microarray study on the impact of UV light exposure of *S. solfataricus* cells (Fröls *et al*., 2007). These genes belonged to a cluster, and possibly an operon of five genes (*sso0117* through *sso0121*) all of which were strongly induced with a maximal induction of 14-fold for *sso0118* (Fröls *et al*., 2007). The transcriptional increases were observed at 1.5–5 h after UV treatment. Over the time-course of 8.5 h, a similar transcriptional reaction pattern for these genes was observed, but not for the upstream or downstream flanking genes (*sso0116* and

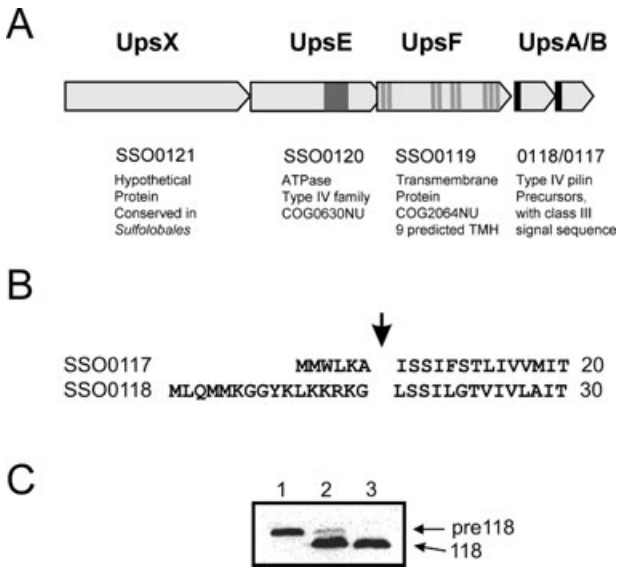

Fig. 1. A. Composition and characteristics of the *ups* operon (UV-inducible pili operon of *Sulfolobus*). Transcriptional induction after UV treatment has been shown in Fröls *et al.* (2007). TMH, transmembrane helices.
B. N-termini of UpsA/B (SSO0117/118) with processing site of PibD indicated by an arrow.
C. Result of *in vivo* cleavage assay of SSO0118-HA by PibD in *E. coli*. Expression of the protein was detected by Western blot analysis using HA-tag antibodies. Lane 1: expression of SSO118-HA in the absence of PibD; lane 2: 2 h after arabinose induction; lane 3: 2 h after induction of PibD by IPTG.

sso0115, *sso0122*). This indicated transcription from a common promoter, as suggested earlier under non-inducing growth conditions (Albers and Driessen, 2005). Only the gene *sso0118* deviated from this UV-dependent pattern and was up to 3.5-fold higher induced, which may indicate the presence of an additional promoter or alternatively, a higher stability of the transcript.

Bioinformatic analysis indicated a putative type IV pili biogenesis operon, represented by a type II/IV secretion system ATPase (SSO0120) and an integral membrane protein (SSO0119) (Fig. 1A). The deduced protein sequence of the ATPase SSO0120 contained Walker A/B sites and a VirB11-related ATPase conserved domain (COG630N). The protein belonged to the TadA subfamily of type IV ATPases (Planet *et al.*, 2001). SSO0119 contained nine predicted transmembrane helices and a TadC (COG2064N) conserved domain. Thus both proteins were homologous to factors of the Tad system (TadA and TadB/TadC), which conveys non-specific tight adherence of *Actinobacillus* on surfaces (Kachlany *et al.*, 2001). The SSO0118 and SSO0117 proteins harboured an N-terminal class III secretory signal sequence as found in type IV pilin precursors. No functional predictions could be made for the first gene, *sso0121*, which encoded a highly hydrophilic protein exclusively found in the genomes of *Sulfolobales*.

The putative pili operon was well conserved in the order *Sulfolobales*, with the same gene arrangement in the strains *Sulfolobus tokodaii* and *S. acidocaldarius* (Table S2 and Szabó *et al.*, 2007b). Further similarities were only found to genes of the hyperthermophilic crenarchaeon *Metallosphera sedula*, belonging to a closely related order. In *M. sedula*, homologues of *sso0120*, *sso0119* and *sso0117* form an operon structure whereas *sso0118* is located in a different genomic region.

Maturation of pre-pilins

Both SS0117 and SSO0118 encode predicted proteins of 15 and 16 kDa, respectively. They contain a signal sequence with the predicted cleavage site for the type IV pre-pilin peptidase PibD (Albers *et al.*, 2003; Szabó *et al.*, 2007b). In SSO0117 and SSO0118 only 6 and 16 amino acids would be cleaved by PibD respectively (Fig. 1B). The ORFs of SSO0117 and SSO0118 were cloned into an *Escherichia coli* expression vector already containing PibD (Szabó *et al.*, 2007b). Using the *in vivo* assay the expression of the pre-pilin proteins was induced for 2 h before the expression of the peptidase was induced. Western blot analysis of crude membrane extracts of the recombinant *E. coli* cells showed that SSO0118 was processed by PibD resulting in a faster running protein species when compared with the full-length protein (Fig. 1C, lanes 2 and 3). Cleavage of SSO0118 was already observed before induction of the expression of PibD, most likely because the promoter used for the expression is leaky and the enzyme cleaves the substrate very efficiently. Cleavage of the signal peptide of SSO0117 could not be observed, most probably because the difference between the precursor and the processed form do not differ enough to be separated on SDS-PAGE. Experiments to separate these two forms in isoelectric focusing gel electrophoresis failed.

UV-induced pili formation

To identify pili, cells were analysed by electron microscopy after UV treatment. To exclude that any extracellular structures were not artefacts of flagella we used the *S. solfataricus* knockout strain Δ*flaJ* that does not produce flagella (Szabó *et al.*, 2007a). Only on the surface of the UV-treated cells, pili-like structures were observed (Fig. 2A). These pili structures were spread over the whole surface and were not polarized at one cell side. Most of the cells of a UV-treated culture contained many pili, some had less or very few (only two to three pili), and few cells did not express pili on their surfaces at all. A time-course experiment showed that the first pili-like structures were observed at 1 h after UV treatment.

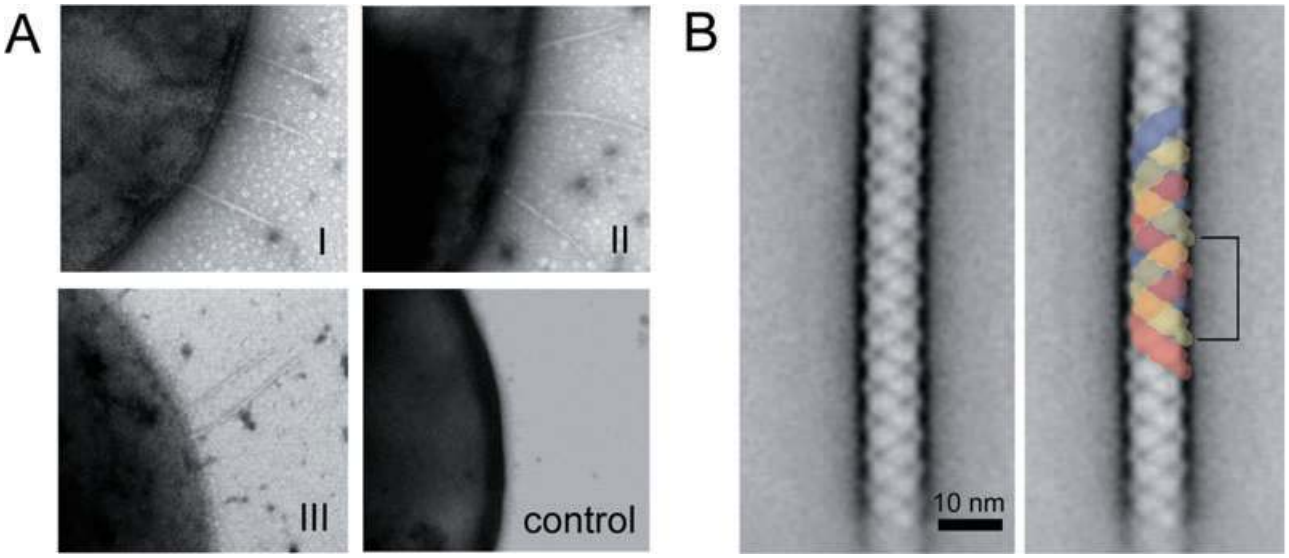

Fig. 2. Electron microscopic analysis of UV-inducible pili in *S. solfataricus*.
A. Δ*flaJ* cells were analysed by electron microscopy 3 h after UV light treatment (I, II and III) and mock treatment for the control.
B. Image processing of pili. Left: projection map obtained after processing 700 non-overlapping fragments of straight pili. Right: Scheme of three-stranded helical arrangement of the pili overlayed. The horizontal lines indicate the pitch of the structure which is 15.5 nm.

In comparison with the flexible flagella, the pili showed a more straight and rigid structure. Pili of up to 16 μm in length or even longer were observed. However, such long filaments where only found detached from the cells, which indicated that they are more fragile than flagella. Because the pili appeared straight for most of their length, it was possible to process them by single-particle analysis selecting straight segments of almost up to 100 nm. About 700 segments were extracted from long pili, aligned and averaged. The final average projection map is shown in Fig. 2B. The structure appeared to consist of three evenly spaced helices. The pitch (repeating unit) of the pili was 15.5 nm and the maximal diameter was about 10 nm. In the negatively stained samples the single helices appeared almost uniformly stained without any clear density differences that could give clues about the handedness (left- or right-handed) of the helices.

Cellular aggregation after UV treatment

The appearance of pili upon UV treatment that could mediate cell-to-cell contacts inspired us to analyse microscopically the formation of cell aggregates (Fröls *et al.*, 2007). We have shown earlier that aggregation occurs with high frequency independent of the *S. solfataricus* genotypes, because experiments with four different strains [P1, PH1, PH1-M16, PH1(SSV1)] showed the same phenotypic reaction. With increasing time after UV treatment, an increasing number of cells were found in aggregates with the highest amount of aggregation found at 6–8 h after UV treatment (Fröls *et al.*, 2007 and Fig. 6). The aggregates increased also in size. While three to five cells were found in the early aggregates, bigger complexes formed at later time points. The shape of the early aggregates seemed to be random, as variations of pyramids, circle shapes, straight and branching chains were observed (not shown). In the later stages (6 h) the cells accumulated to big clusters of >100 cells. As it was impossible to count the number of cells in such aggregates, our quantitative data (% cells in aggregates of total cell count) generally represent an underestimate.

Attempts to destroy the cell–cell connections by shear force experiments resulted in cell lysis at all stages but not in disaggregation, indicating a high stability of the aggregates. The induction of cellular aggregation was UV-dose-dependent (see Fig. 3). We treated the cells with seven different UV doses ranging from 5 to 1000 J m^{-2}. Growth retardation of the respective cultures was directly proportional to the applied UV dose (data not shown). The highest cellular aggregation was observed 6 h after UV treatment, i.e. at the expected maximum. The highest amount of cellular aggregation was found with 75 J m^{-2} (up to 50% and sometimes even 70% of cells in aggregates, Fig. 3A and Fröls *et al.*, 2007) and with 50 J m^{-2} (at least 40% of the cells were in aggregates of ≥ 3 cells, Fig. 3A). Even the lowest dose of UV light of 5 J m^{-2} induced the cellular aggregation, whereas the high UV doses of 200 and 1000 J m^{-2} showed a very low and no significant aggregation reaction respectively. We also observed a strong correlation between the size and amount of cellular aggregates (Fig. 3B). Low doses of 5 and 10 J m^{-2} resulted in cellular aggregates of <7 cells.

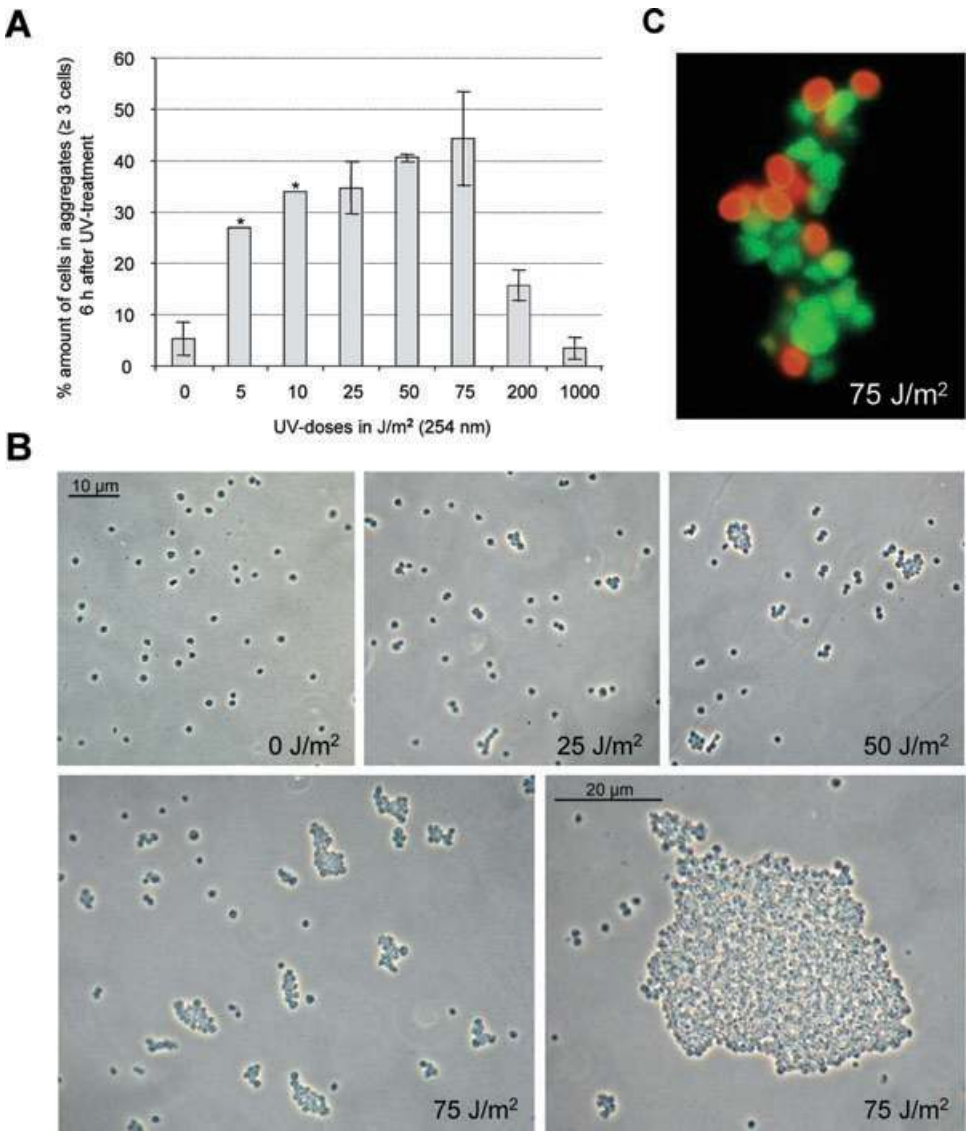

Fig. 3. Aggregation of *S. solfataricus* cells after treatment with different UV doses.
A. Quantitative analysis of cellular aggregation at 6 h after UV treatment. Exponential cultures were treated with 0, 5, 10, 25, 50, 75, 200 and 1000 J m^{-2}. The percentage amount of cells in aggregates (≥ 3 cells) is given in relation to the total cells. For each UV dose the amount of cells in and outside aggregates were counted until 500 single cells were found. The bars display the mean of three independent experiments, except for 5 and 10 J m^{-2} (see asterisk), where only one experiment was performed.
B. Light micrograph of *S. solfataricus* cell aggregates at 6 h after UV treatment with different UV doses. The size of the aggregates increased with the UV dose; the biggest aggregates were found after treatment with 50 and 75 J m^{-2}.
C. Fluorescence micrograph of a *S. solfataricus* cell aggregate at 6 h after UV treatment at 75 J m^{-2}. Cells were stained with the LIVE DEAD Baclight (Invitrogen) assay. Living cells are labelled in green and dead cells in red. Big aggregates of > 20 cells were mostly found at 3 h after treatment. For quantitative analysis of the cell vitality at different UV doses see Table 1.

Only upon a UV dose of 50–75 J m^{-2}, large aggregates of 10–20 cells or many more were generated frequently. Because cells in these biggest aggregates could not be counted, our numbers in Fig. 3A represent an underestimate for 50 and 75 J m^{-2}. In the case of the high UV doses of 200 and 1000 J m^{-2} no aggregates > 4 cells were observed.

By using different vital staining techniques (see *Experimental procedures*), we investigated whether dead cells accumulate in aggregates (see Table 1). In the case of the lowest UV dose of 5 J m^{-2} only 8% of the total cells in aggregates (≥ 3 cells) were dead. The amount of dead cells increased proportionally with the UV dose but was far lower than the number of living cells. The majority of the cells (64%) present in the infrequent aggregates at 200 J m^{-2} were not alive. At lower UV dose, like 75 J m^{-2}, even large aggregates of > 20 cells were almost uniformly composed of living cells (Fig. 3C).

Table 1. Cell vitality of *S. solfataricus* cells in aggregates formed after treatment with UV light.

UV dose (J m^{-2})	Vital cells in %[a]
5	92
10	88
25	83
50	66
75	56
200	36

a. At 6 h after UV treatment a live and dead stain was performed (see *Experimental procedures* and also Fig. 3C).
A minimum of 50 aggregates ≥ 3 cells were counted per each UV dose and the fraction of vital cells is given in relation to the total cells found in aggregates.

Gene knockout in the UV-inducible pili operon abolishes pili formation and cellular aggregation

To prove that pili were indeed assembled from components expressed from the putative pili operon, a deletion mutant was constructed in which the ATPase (*sso0120*) was replaced by insertion of a *lac*S cassette containing the *lacS* gene with its natural promoter and terminator region via a double cross-over. The successful deletion of the *sso0120* gene was confirmed by Southern analysis and RT-PCR (see Fig. 4A and B). The RT-PCR showed that under inducing conditions the *sso0120* mRNA was absent, while the downstream genes of the operon were still expressed, probably because of readthrough of the *lac*S terminator by the RNA polymerase. After UV treatment of the mutant Δ*sso0120* we could not observe any pili-like structures on the cellular surfaces by electron microscopy (Fig. 4C, Ia and Ib). As control, we used the parent strain PBL2025 (Schelert *et al.*, 2004) which clearly showed pili-like structures beside the flagella upon exposure to UV light (Fig. 4C, IIa and IIb). When the mutant strain Δ*sso0120* was complemented with pSVA99 containing *sso0120* under the control of the *araS* promoter, pili were again observed after UV treatment, but only when the cells were additionally incubated with arabinose (Fig. 5A). Overexpression of both pilin genes, *sso0117* and *sso0118*, in the Δ*flaJ* strain using the virus-based vector construct pSVA96 resulted in the assembly of fewer, but extremely long and irregular pili (Fig. 5B). The overexpression of the whole operon, *sso0121-0117*, using pSVA125 led to the formation of pili around the whole cell surface (Fig. 5C), whereas the expression of a cytoplasmic control protein from pSVA31 did not result in the assembly of surface structures (data not shown). Together these data demonstrate that formation of the pili is dependent on expression of *sso0120* and that the two pre-pilins (or one of them) most likely form the subunits of the UV-inducible pili.

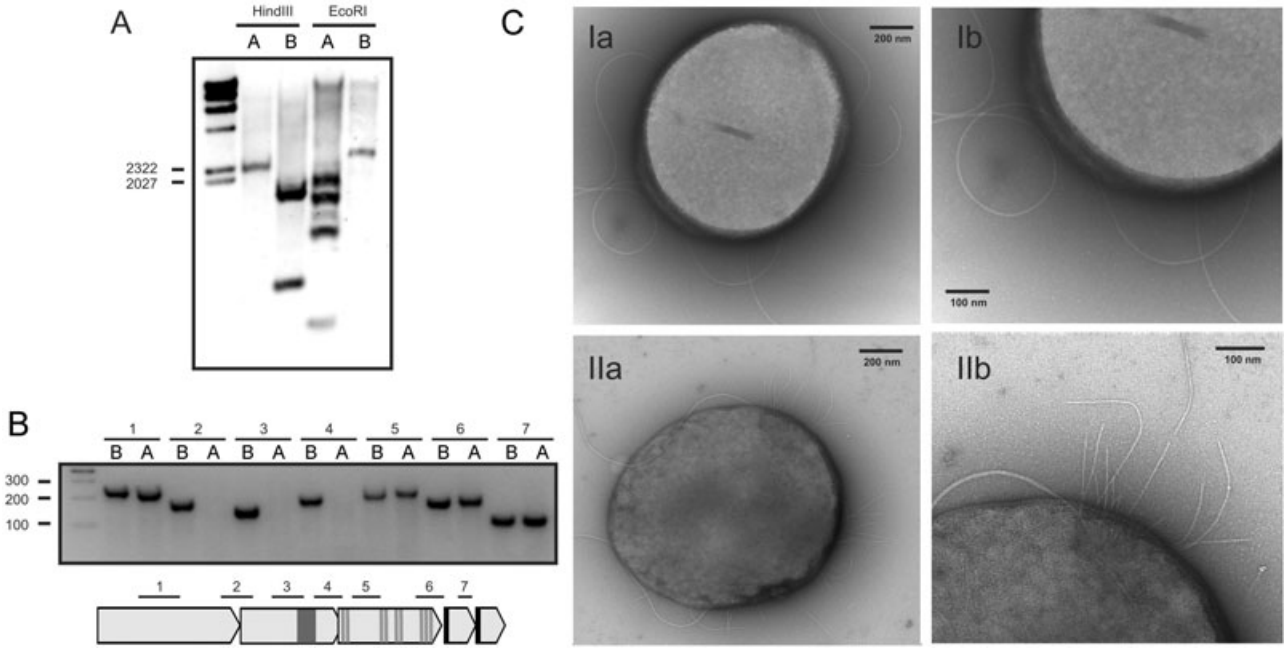

Fig. 4. Analysis of the *sso0120* knockout strain.
A. Southern blot analysis of wild-type PBL2025 (B) and the Δ*sso0120* (A) strain. Genomic DNA was each digested with HindIII or EcoRI respectively.
B. RT-PCR analysis of PBL2025 (B) and Δ*sso0120* (A) strain after UV stress. The position of the primers used for the PCR reactions are indicated by the same number above the gel and the map of the operon.
C. Electron micrographs 3 h after UV treatment. Only long flagellar but no pili can be observed in the Δ*sso0120* strain (Ia and b) while the surface *of* PBL2025 (IIa and b) is covered with pili.

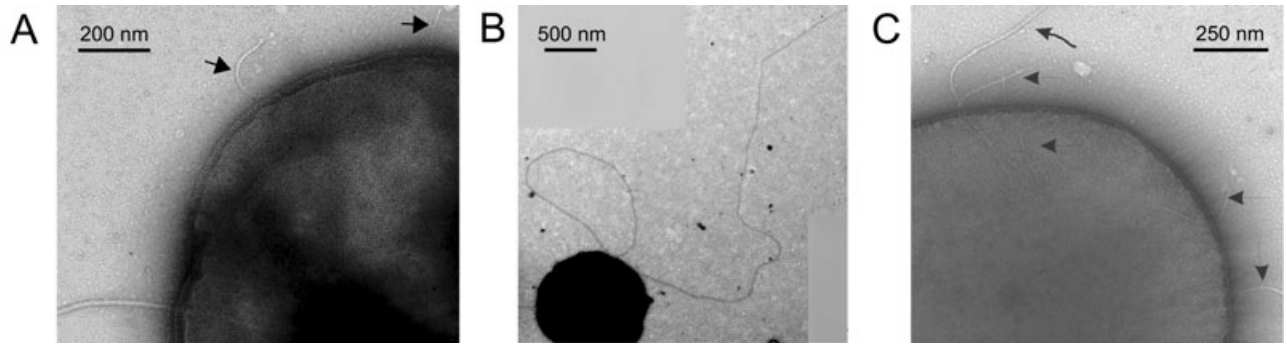

Fig. 5. Electron micrographs of *S. solfataricus* cells assembling pili. (A) shows a UV-treated Δ*sso0120* cell expressing *sso0120* under the control of the *araS* promoter. (B) depicts a Δ*flaJ* cell overexpressing the pilins SSO117/118 and overexpressing the whole operon comprising SSO0121-117 (C). In (B) two pictures were assembled to show the length of the pilus; in (A) and (C) pili are indicated by the arrows.

The Δ*sso0120* strain was further tested for its ability to form cellular aggregates upon UV exposure. After a treatment with a UV dose of 50 J m^{-2} no significant cellular aggregation of more than four cells was observed (Fig. 6). The amount of cells in aggregates accounted for less than 10% in the UV-treated culture and the control (mock-treated) culture, similar to the amount of cells in aggregates observed for the mock-treated cultures of the other four tested *S. solfataricus* strains. The *S. solfataricus* strain P1 and PH1-M16 (P1 Δ*lacS*) showed a maximum aggregation at 6–8 h after treatment, with an average of 45–50% cells in aggregates. In the same experiment, the PBL2025 and the Δ*flaJ* strains exhibited a shifted maximum at 8–10 h and a lower amount of aggregation with an average of 20%. The weaker reaction is most probably due to the different genotypes of these strains, which stem from PBL2025, an isolate from Yellowstone National Park *S. solfataricus* 98/2s (Schelert *et al.*, 2004). Comparable results were observed when using a lower UV dose of 25 J m^{-2} (see Fig. S1). Again, no significant cellular aggregation was observed for strain Δ*sso0120*. The P1 and PH1-M16 strains showed a lower amount of aggregation with 30–40%, as expected in relation to the lower UV dose. The amount of cells in aggregates in the case of the PBL2025 strain stayed the same, whereas with the Δ*flaJ* strain the amount of cells in aggregates increased to > 30% and the maximum shifted to 6 h. Based on these results we conclude that the UV induction of the putative pili operon, the inducible pili production and the cellular aggregation are functionally linked to each other. We therefore named the newly identified operon UPS for UV-inducible (type IV-like) pili operon of *Sulfolobus*, represented by the genes *upsX*, *upsE* (ATPase), *upsF* (TM protein), *upsA* and *upsB* (pre-pilins).

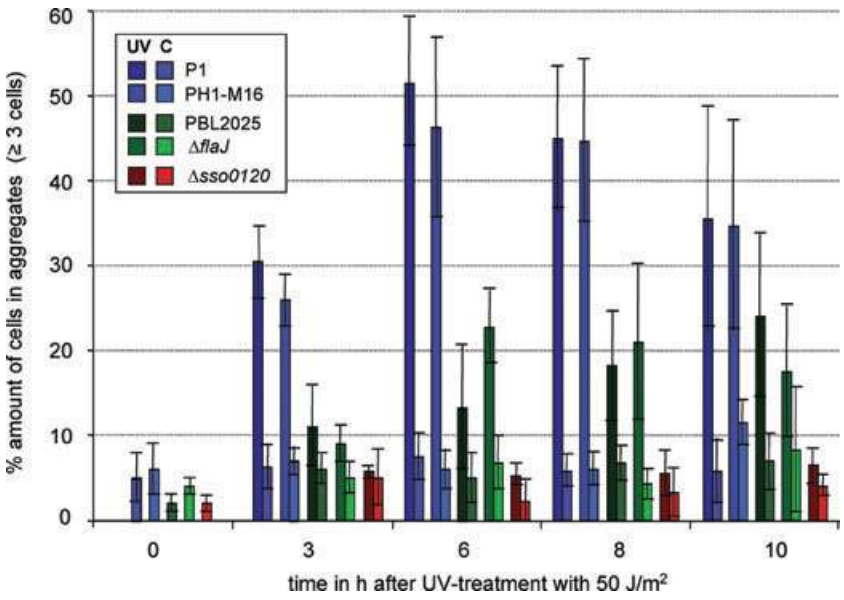

Fig. 6. Quantitative analysis of the UV-induced cellular aggregation of different *S. solfataricus* strains at 0–10 h after UV treatment (UV) and mock treatment (C). The graph is based on four independent UV experiments for each strain. Cellular aggregation was observed at 3, 6, 8 and 10 h after UV treatment with 50 J m^{-2} (254 nm). The bars display the percentage amount of cells in aggregates (≥ 3 cells) in relation to the total amount of evaluated cells (500–1000 single cells were counted).
No UV-induced cellular aggregation was observed in the knockout strain Δ*sso0120*. Similar results were observed by using a UV dose of 25 J m^{-2} (254 nm) displayed in Fig. S1.

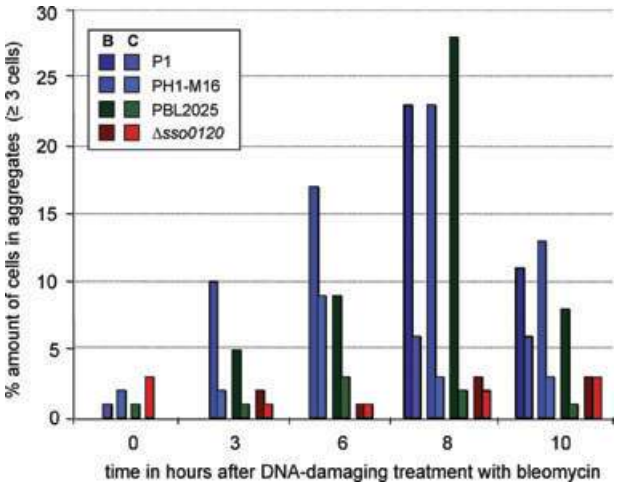

Fig. 7. Aggregate formation of different *S. solfataricus* strains after treatment with bleomycin (B) (3 μg ml^{-1}) and mock treatment (C). No significant cell aggregation was observed with the knockout strain Δ*sso0120*. The bars display the percentage amount of cells in aggregates (≥ 3 cells) in relation to the total amount of evaluated cells (500 single cells were counted).

Cellular aggregation is not inducible by other environmental stressors or in late growth phases

To analyse if cellular aggregation can be induced by conditions other than UV exposure, four strains that harbour the wild type of the *ups* operon were used: *S. solfataricus* strains P1, PH1-M16, PBL2025 and Δ*flaJ*. We monitored and quantified the extent of cellular aggregation after a temperature shift from 78°C to 88°C (heat shock) and down to 65°C (Kagawa *et al.*, 2003), which corresponded to non-lethal heat- and cold-shock conditions that might be often encountered in hot springs. Shifts from pH 3 to 4 and down to pH 2.5 were similarly investigated. No significant cellular aggregation was observed under the tested conditions in any of the four tested strains. The amount of cells in aggregates (≥ 3 cells) was always below 10% (see Fig. S2). We also monitored the extent of cellular aggregation in the late growth phases of the cultures, from stationary to dead phase. Only at the beginning of the late stationary phase, i.e. at the start of growth retardation, a slightly increased cellular aggregation was noted. For strain P1 up to 24% of the cells were found in aggregates of four to seven cells at most, while the amount of cells in aggregates (≥ 3 cells) were lower than 10% in all other growth phases (see Fig. S2).

Cellular aggregation is induced by treatment with DNA double-strand breaking-inducing agents

As a response of *S. solfataricus* to UV light we observed earlier the formation of DSB in the genomic DNA (Fröls *et al.*, 2007). Whereas *cis*-syn-cyclobutane pyrimidine dimers (CPDs) represent direct DNA damages caused by the UV light effect, DSB are probably formed as a result of collapsing replication forks at unrepaired sites in the genomic DNA. It has been speculated earlier that DSB might represent an intracellular signal for further cellular reactions. Therefore we determined whether the formation of DSB is connected to the formation of cellular aggregates. The induction of cellular aggregation of the different *S. solfataricus* strains P1, PH1-M16, PBL2025 and Δ*sso0120* in response to the DSB-inducing agents bleomycin (3 μg ml^{-1}) (Fig. 7) and mitomycin C (5, 10 and 15 μg ml^{-1}) was investigated (Cannio *et al.*, 1998; Reilly and Grogan, 2002; Kosa *et al.*, 2004) (Table 2). The concentrations we applied were non-lethal to the cells as investigated by plating efficiencies and growth behaviour in liquid cultures (data not shown). Cellular aggregation was monitored at 3, 6 and 8 h after the treatment and with bleomycin additionally at 1 and 10 h. All tested strains, except for the Δ*sso0120* strain, showed a significant cellular aggregation in response to the agents. Eight hours after the treatment with bleomycin, strains P1, PH1-M16 and PBL2025 exhibited 25–35% of cells in aggregates (Fig. 7), while aggregation in the mock-treated cultures and the bleomycin-treated strain Δ*sso0120* remained below 10%. Similarly, although less strongly, mitomycin C induced aggregate formation in the *ups* operon containing wild-type strains (P1, PBL2025), but not in the knockout strain (Table 2). These observations indicate that DNA damage and in particular DSB might be a direct or indirect signal for inducing aggregate formation.

Discussion

The special living conditions of *Archaea* in extreme environments make them interesting objects to study adaptations and stress responses. In particular hyperther-

Table 2. Cellular aggregation in percentage after treatment with mitomycin C.[a]

Strain	Mitomycin C dose	Time in hours after treatment		
		3 h	6 h	8 h
P1 (wild-type strain)	5 μg ml^{-1}	5	10	10
	10 μg ml^{-1}	8	10	16
	Control	1	2	2
PBL2025	5 μg ml^{-1}	1	10	9
	15 μg ml^{-1}	6	12	10
	Control	1	1	3
PBL2025:Δ*sso0120*	5 μg ml^{-1}	1	1	2
	15 μg ml^{-1}	0	0	0
	Control	0	1	0

a. The percentage amount of cells in aggregates (≥ 3 cells) in relation to the total number of evaluated cells is given (a minimum of 500 single cells were counted).

mophilic and acidophilic *Archaea* like *S. solfataricus* have to deal with a constant stress and DNA damage in their harsh environments. Here we present the identification and characterization of an archaeal pili system that mediates cellular aggregation of *S. solfataricus* in response to UV damage. The genes encoding the now called *ups* operon for UV-inducible (type IV-like) pili operon of *Sulfolobus* had earlier been identified to be UV-dependently induced in a genome-wide DNA microarray analysis (Fröls *et al*., 2007).

To our knowledge this is the first reported study on a UV-inducible pili-mediated auto-aggregation system. As discussed below, its induction seems to be coupled to the DNA DSB caused by UV irradiation. We suspect that cellular aggregation mediates DNA repair via a conjugation-like process, as an enhanced exchange of chromosomal markers has been observed upon UV irradiation as well as increase in the transcripts levels of genes involved in homologous recombination.

UV-inducible pili mediate cellular aggregation

By electron microscopic analysis we found a strong correlation between the formation of extracellular pili on the cellular surface after UV treatment and the expression of the *ups* operon, both of which appeared first at 1 h after UV treatment and reached a maximum within 5–6 h. To test our hypothesis that the gene products of the *ups* operon are responsible for the production of the pili we used the recently developed genetic system (Albers and Driessen, 2007) to produce a specific knockout of the putative secretion ATPase UpsE (SSO0120). No pili structures were observed on the cellular surface of the Δ*sso0120* strain. By testing this strain in a quantitative cellular aggregation analysis, we proved that the pili are necessary for the cellular aggregation of *S. solfataricus* after UV treatment. Cellular aggregates were as infrequent (i.e. lower than 10% of all cells) as in mock-treated controls of four different *S. solfataricus* strains. Image analysis of isolated pili structures showed that the pili are much thinner in diameter and clearly distinguishable from the flagella of *S. solfataricus* (Szabó *et al*., 2007a). A detailed structural analysis of another archaeal pilus has recently been published from a methanogenic euryarchaeote *Methanococcus maripaludis* (Wang *et al*., 2008).

The pili-like structures of *S. solfataricus* are spread over the whole cellular surface. They are not bundled or polarized like the cable-like flagellar bundles of *P. furiosus*, which mediate cell attachment (Näther *et al*., 2006) or the type IV pili of the Tad system from *Actinobacillus* species that mediate non-specific adherence (Kachlany *et al*., 2000; 2001). Experiments to disconnect cellular aggregates by shearing forces failed, indicating that the cell–cell contacts were highly stable once formed and showing that the cellular aggregates were not a result of an unspecific accumulation. The latter was also ruled out by a live and dead stain analysis (Fig. 3C and Table 1). The detailed mechanisms of auto-aggregation is, however, still unknown. It has been reported that the bacterial type IV pili are bound with their tip on surface structures or other cells (Mattick, 2002). So far, we did not observe any attachment to surfaces. However, our experiments were performed under moderate shaking in glass flasks, such that one cannot rule out the possibility of surface attachment under different conditions.

UV-inducible cellular aggregation is highly dynamic

A quantitative assay was developed in this study to analyse the dynamics of cellular aggregation in more detail. We showed that the aggregation is a fast process induced by the UV-dependent reaction of *S. solfataricus* and seems to occur in two phases. First, small aggregates of three to five cells accumulate, which later aggregate to larger forms. The maximum of aggregation was reached at 6–8 h after UV treatment, followed by a clear disappearance, interpreted as an active disaggregation. One has to note that the absolute amount of cellular aggregation is by far underestimated because cell aggregates of more than 20 cells were uncountable and the biggest aggregates with even up to 100 and more cells were found frequently at 6 h after UV treatment. Furthermore, cell aggregates of two were not incorporated in the calculations in order to exclude dividing cells.

In correlation to the cell cycle length of *S. solfataricus*, which is around 7 h, the dynamics of this process are relatively fast. For example, the cellular packets of *M. mazei* need 2–6 days to form the lamina structures, and then remain stable over 6–11 days until the culture reaches stationary growth phase and the lamina disaggregate (Mayerhofer *et al*., 1992). The stress induced biofilm formation of *A. fulgidus* occurs in 2–12 h, but in this case no disaggregation was reported (LaPaglia and Hartzell, 1997).

UV light is the only identified stressor to induce auto-aggregation

It is reported that cells organized in multicellular structures show a higher resistance to different environmental stressors, like temperature, pH and also UV light (Ojanen-Reuhs *et al*., 1997; Roine *et al*., 1998; Martinez and Casadevall, 2007). Treatment of the hyperthermophilic archaeon *A. fulgidus*, with a high dose of UV light and other physical or toxic stressors, results in a biofilm production (LaPaglia and Hartzell, 1997). Mutants of plant pathogen bacteria *Pseudomonas syringae* and *Xan-*

thomonas campestris defect in the auto-aggregation showed a higher sensibility to UV irradiation than the wild type capable of forming multicellular structures (Ojanen-Reuhs *et al*., 1997; Roine *et al*., 1998). A decreased sensitivity to UV light and other environmental stressors was also reported for biofilms of the yeast-like fungi *Cryptococcus neoformans* (Martinez and Casadevall, 2007). None of the stressors that we used for *S. solfataricus* induced cellular aggregation, nor did late growth phase stages. This stands in contrast to all given examples of multicellular structures, which are typically interpreted as an advantageous life form under harsh or specialized environmental conditions. Thus *S. solfataricus* shows a unique multicellular formation which is not a general effect of a stress response.

Interestingly, the extent of cellular aggregation (aggregate sizes and the number of cells involved) was dependent on the UV dose. Relatively high doses of UV light, like 200 or 1000 J m^{-2}, resulted in an insignificant amount of small aggregates ($\leq$ 4 cells) and killed most of the cells. In contrast a relatively low dose of UV light, like 5 J m^{-2}, induced cellular aggregation. In nature sunlight composed of up to about 96% UV-A reaches the ground with *c*. 4% UV-B that is the most DNA-damaging factor. The daily dose of DNA-damaging UV-B light on a sunny day in the northern and southern world hemispheres is measured between 1000 and 3000 J m^{-2} over 24 h (depending on the season). The experimentally used UV-C (254 nm) is about 100-fold more effective than UV-B in inducing CPDs (Kuluncsics *et al*., 1999). With reference to the observation that even low dose of UV light significantly induces the cellular aggregation of *S. solfataricus* we conclude that this phenotypic effect reflects the behaviour of the organism to the sunlight in the natural environment.

Cellular aggregation is induced by DNA DSB and might mediate a recombinational repair among chromosomes of mating cells

Between 2 and 8 h after UV treatment we observed the formation of DNA DSB, probably resulting from replication fork collapse at damaged DNA sites (Fröls *et al*., 2007). These observations inspired us to investigate in this study if the cellular aggregation is causally linked to the presence of DSB in the genome. Indeed, the DSB-inducing agents bleomycin and mitomycin C caused the same phenotype of cellular aggregation as UV light. Similarly, the proliferation of the *S. shibatae* virus 1 (SSV1) can be induced by mitomycin C as well as UV light (Martin *et al*., 1984) indicating that the same internal signal cascades are involved.

However, it is still unclear how DSB DNA might be sensed in the cells and how the signal is further transferred to induce the cellular aggregation and DNA-repair reactions. A phototaxis mechanism is reported for *H. salinarum* that regulates the motor switch of the flagella. The UV light is sensed by the sensory rhodopsin (Htr) and activates a Che-like two-component system (Nutsch *et al*., 2003). However, neither of these components is known in *Sulfolobales*. In *Synechocystis* PCC6803 Che-like histidine kinases control the cell orientation to the light and type IV pilus biosynthesis (Bhaya *et al*., 2001).

We observed that strain Δ*sso0120* was more sensitive than wild type to DSB-inducing agents, suggesting that cell aggregation is required for efficient DNA repair. Although aggregation could simply reduce the exposure of cells to UV light by shading, we believe that aggregation might play a role in mediating the formation of mating pairs that allow DNA repair via homologous recombination among the partners.

Significantly enhanced exchanges of chromosomal markers upon treatment with UV light have been described for *Sulfolobus* (Wood *et al*., 1997; S. Fröls and C. Schleper, unpublished).

Furthermore, we found a slight, but significant upregulation of the *mre11* operon upon UV treatment in *S. solfataricus* using whole-genome microarrays (Fröls *et al*., 2007). This operon encodes homologues of the eukaryotic system involved in the DSB repair via homologous recombination (Hopfner *et al*., 2002; Constantinesco *et al*., 2004).

By integrating our observations and those cited above we think that recombinational repair via homologous recombination and DNA exchange via cell–cell contacts might be an important strategy to overcome DNA damage in *Sulfolobus* caused by UV light. Future studies will aim at investigating if this is indeed the case. It will also be interesting to elucidate the transcriptional regulation of the UV-induced genes, with the perspective to clarify the signal transduction pathways that sense UV irradiation or DNA damage in crenarchaeota.

Experimental procedures

Strains and growth

Sulfolobus solfataricus P1 (DSM1616), PH1 (Schleper *et al*., 1994), PH1-M16 (Martusewitsch *et al*., 2000) and PBL2025 (Schelert *et al*., 2004) and derived deletion mutants were grown aerobically at 80°C in the medium described by Brock *et al*. (1972), adjusted to pH 3 with sulphuric acid and supplemented with 0.1% (w/v) of trypton and 0.2% (w/v) of arabinose under moderate agitation (150 r.p.m. in a New Brunswick shaker). Growth of cells was monitored by measuring the optical density at 600 nm. Solid media were prepared by adding gelrite to a final concentration of 0.6% and $MgCl_2$ and $CaCl_2$ to 0.3 and 0.1 M respectively. Plates were incubated for 5 days at 78°C. For the propagation of plasmids, *E. coli* strain DH5α was used. For the virus containing

Table 3. Plasmids used in this study.

Plasmid name		Reference
pET2268	Vector containing *lacS* cassette	Szabó *et al.* (2007b)
pZA7	Transfer vector to add HA-tag to proteins	Szabó *et al.* (2006)
pUC18-*pibD*	pUC18 containing pibD under the control of a T7 promoter	Szabó *et al.* (2007a)
pMZ1	Entry vector for virus vector	Zolghadr *et al.* (2007)
pMJ05[a]	Virus-based shuttle vector for *S. solfataricus*	Jonuscheit *et al.* (2003)
pSVA31	pMJ05 containing *ABCE1* under control of *araS* promoter	Albers *et al.* (2006)
pSVA37	pET2268 containing up- and downstream flanking regions of *sso0120*	This study
pSVA96	pMJ05 containing *sso117/118* under control of *araS* promoter	This study
pSVA99	pMJ05 containing *sso0120* under control of *araS* promoter	This study
pSVA125	pMJ05 containing *sso121-117* under control of *araS* promoter	This study
pSVA133	pZA7 containing *sso0118*	This study
pSVA134	pBAD/*Myc*-HisA containing *sso0118*-HA	This study
pSVA135	pSVA134 containing *pibD*	This study

a. Plasmids labelled bold are shuttle vectors for *S. solfataricus/E. coli*.

plasmids ElectroMAX™ *E. coli* Stbl4™ cells (Invitrogen, Germany) were used.

UV light exposure

UV treatment of cells was performed under red dimmed light. Aliquots of 10 ml of *S. solfataricus* culture (OD_{600} 0.3–0.5) were transferred to a 110 mm plastic Petri dish and treated with a defined UV dose (λ 254 nm, UV-Stratalinker 1800, Stratagene). Treated cell suspensions were combined to a final volume of 20 ml. The mock-treated cultures were set for 5 s under red dimmed light. Treated cells were stored in the dark at room temperature for 15 min and were re-incubated at 78°C and 150 r.p.m. Samples taken at different time points were used for microscopy, cell vitality and electron microscopy.

Electron microscopy and single-particle analysis

For image processing, cells with attached pili were negatively stained with 2% uranyl acetate on glow-discharged carbon-coated copper grids. Electron microscopy was performed on a Philips CM120 electron microscope operating at 120 kV with a LaB6 filament. Images were recorded with a 4000 SP 4K slow-scan CCD camera at 60 000× magnification at a pixel size of 5.0 Å at the specimen level with 'GRACE' software (Oostergetel *et al.*, 1998). Single-particle analysis was performed with the Groningen Image Processing ('GRIP') software package on a PC cluster. Non-overlapping pili segments were extracted from the micrographs and aligned with correlation methods. The aligned projections were treated with multivariate statistical analysis in combination with hierarchical classification before final averaging (van Heel *et al.*, 1992; Penczek *et al.*, 1992).

Plasmid construction for expression in S. solfataricus *and* E. coli

The genes *sso0117* and *sso0118* were cloned using primers 118-forward-NcoI and 117-reverse-BamHI in the same arrangement as found in the genomic context into the virus-based expression vector pMJ05 (Jonuscheit *et al.*, 2003) via the entry vector pMZ1 (Zolghadr *et al.*, 2007) yielding pSVA96. To express the whole *ups* operon genes *sso0121-117* were cloned using primers 121-forward-NcoI and 117-reverse-BamHI via pMZ1 into pMJ05 resulting in pSVA125. To construct the expression plasmid for the signal peptide cleavage assay, *sso0118* was amplified using 118-forward-NcoI and 118-reverse-BamHI and cloned into pZA7, which added a HA-tag to the C-terminus of the protein and resulted in pSVA133. By NcoI–HindIII restriction the sso0118-HA part was then transferred into pBAD/Myc-HisA yielding pSVA134. To achieve coexpression with the peptidase a fragment containing *pibD* under the control of the T7 promoter was cloned from pUC18-pibD into pSVA134 by SphI restriction resulting in pSVA135. All plasmid vectors used in this study are listed in Table 3.

For the expression of SSO117/118 and the *ups* operon in the Δ*flaJ* strain, cells were grown to an OD_{600} of 0.2, and transformed with pSVA96, pSVA125 and pSVA31 as a control as described by Jonuscheit *et al.* (2003). After 2 days, cultures were transferred to medium containing 0.4% arabinose to induce the expression of the desired genes. After one transfer, cells were analysed at an OD_{600} of 0.7 cells by electron microscopy.

Construction of plasmids for the directed deletion of genes

The up- and downstream flanking regions of *sso0120* were amplified using primer pairs KO-UP forward/KO-UP reverse and KO-DOWN forward/KO-DOWN reverse respectively (Table S1). The resulting fragments were cloned using KpnI/NcoI for the upstream flanking region (1099 bp) or BamHI/NotI for the downstream flanking region (924 bp) in pET2268, a vector containing the *lacS* cassette for selection, yielding pSVA37. Electroporation of the knockout plasmids and selection for correct deletion mutants were performed as described (Albers and Driessen, 2007).

Southern blotting

Genomic DNA (8 ng) was digested with the appropriate enzymes and separated on 0.8% agarose gel. The gel was

equilibrated in 20× SSC and the DNA was transferred overnight to a positively charged nylon membrane (BIO-RAD, the Netherlands). DNA hybridization was performed in standard hybridization buffer. PCR products of both *lacS* and the *sso0120* gene were digoxigenin-labelled with the HighPrime Kit (Roche, the Netherlands). Detection was performed with a LumiImager (Roche, the Netherlands).

Gene expression analysis

Total RNA isolation and cDNA synthesis were performed as described previously (Zolghadr *et al.*, 2007). Gene-specific primer sets (1–7, Table S1) were used to detect the presence of the genes in the *ups* operon. PCR products were analysed on 0.8% agarose gels.

Isolation of E. coli *crude membranes*

BL21(DE3) (pLysS) *E. coli* cells were transformed with plasmids pSW017, pSW018, pSW019 and pSW020. The signal sequence cleavage assay was performed as described before (Szabó *et al.*, 2007b). At an OD_{600} of 0.6, the expression of the precursor genes, *sso0117/118*, was induced by addition of 0.2% L-arabinose for 2 h. Subsequently, the expression of *pibD* was induced with 0.1 mM isopropyl-beta-D-thiogalactopyranoside (IPTG) for 2 h. The cultures were harvested, and cell pellets were re-suspended in 2 ml of buffer (50 mM TrisCl, pH 7.5, 1 mM EDTA). Crude membranes were isolated as described previously (Szabó *et al.*, 2007b) and re-suspended in 50 mM TrisCl, pH 7.5. Cleavage of substrates was determined by SDS-PAGE and Western blot analysis of 5 μg of crude membranes using monoclonal anti-haemagglutinin (HA Tag) antibodies (Sigma).

Microscopy and quantitative analysis of cell aggregate formation

Cell aggregate microscopy was performed as described (Fröls *et al.*, 2007). To quantify the formation of aggregates, the number of cells in aggregates and the number of aggregates were counted until 1000 or 500 single cells were observed. At least seven fields of views were analysed for each time point. To exclude that the cellular aggregates were not artefacts of the microscopic slide preparation only fields of views were analysed where the cells showed an even spreading. For statistic analysis the percentage of cells in aggregates ≥ 3 cells (to exclude the dividing pairs of cells) against the total amount of cells was calculated. Additionally the percentage of each aggregates size (from 3 to 15 cells) against the total amount of cells was determined to observe the time- and dose-dependent formation of cellular aggregates in a higher resolution.

Analysis of the cell viability

To analyse the cell viability the LIVE DEAD Baclight (Invitrogen) assay was used according to the manufacturer's instructions. Alternatively, a combined 4′,6-diamidino-2-phenylindole (DAPI) propidium iodide stain was used. At 6 h after UV treatment, samples of 20 μl of liquid cultures were mixed with 2 μl of propidium iodide (1:30 dilution in 10 mM TrisCl pH 7.5) and incubated for 15 min in the dark at room temperature. Microscopic slides were coated with 1% agar (10 mM TrisCl, pH 7.5) containing 0.2 μg ml^{-1} DAPI. Propidium iodide-stained culture (5 μl) was spread on the coated slide and immediately examined. To analyse the number of dead cells in aggregates in relation to the living cells, a minimum of 50 cellular aggregates of ≥ 3 cells were counted for each UV dose.

Testing of various stress factors

For the temperature shift, exponentially grown *S. solfataricus* cultures (OD_{600} of 0.3–0.5) were transferred from 78°C to 88°C or to 65°C. Additionally control cultures were transferred to 78°C with gentle shaking at 150 r.p.m., and at time points up to 10 h after transfer, samples were analysed for aggregation.

For the pH shift experiments, exponential-grown *S. solfataricus* cells were harvested and re-suspended in an identical volume of Brock's basal salt medium supplemented with D-arabinose (0.2%) and tryptone (0.1%) at pH values of 2.5, 3 and 4 respectively. Growth was continued at 78°C. Samples for the quantitative analysis of the cellular aggregation were taken up to 8 h after the pH shift. For the treatment with the DSB-inducing antibiotics, an exponential *S. solfataricus* culture was treated with 3 μg ml^{-1} bleomycin (Bleocin, Calbiochem) or 5, 10 and 15 μg ml^{-1} mitomycin C (Sigma). Growth was continued at 78°C and cell samples taken up to 10 h after antibiotics additions were plated on Brock's solid media. Survival rates confirmed the use of a non-lethal drug concentration for both antibiotics as described (Cannio *et al.*, 1998; Reilly and Grogan, 2002; Kosa *et al.*, 2004).

Acknowledgements

The work has been funded by Deutsche Forschungsgemeinschaft within SPP1112 and by the University of Bergen. D.T. is funded by the Marie Curie research training network MRTN-CT-2006-033499. S.-V.A. and B.Z. were supported by a VIDI grant from the Dutch Science Organization (NWO). M.A. was funded by an Ubbo-Emmius scholarship of the University of Groningen.

References

Albers, S.V., and Driessen, A.J.M. (2005) Analysis of ATPases of putative secretion operons in the thermoacidophilic archaeon *Sulfolobus solfataricus*. *Microbiology* **151:** 763–773.

Albers, S.V., and Driessen, A.J.M. (2007) Conditions for gene disruption by homologous recombination of exogenous DNA into the *Sulfolobus solfataricus* genome. *Archaea* **2:** 145–149.

Albers, S.V., Szabó, Z., and Driessen, A.J.M. (2003) Archaeal homolog of bacterial type IV prepilin signal peptidases with broad substrate specificity. *J Bacteriol* **185:** 3918–3925.

Albers, S.V., Jonuscheit, M., Dinkelaker, S., Urich, T., Kletzin,

A., Tampé, R., *et al.* (2006) Production of recombinant and tagged proteins in the hyperthermophilic archaeon *Sulfolobus solfataricus*. *Appl Environ Microbiol* **72:** 102–111.
Bardy, S.L., and Jarrell, K.F. (2002) FlaK of the archaeon *Methanococcus maripaludis* possesses preflagellin peptidase activity. *FEMS Microbiol Lett* **208:** 53–59.
Battin, T.J., Sloan, W.T., Kjelleberg, S., Daims, H., Head, I.M., Curtis, T.P., and Eberl, L. (2007) Microbial landscapes: new paths to biofilm research. *Nat Rev Microbiol* **5:** 76–81.
Bhattacharjee, M.K., Kachlany, S.C., Fine, D.H., and Figurski, D.H. (2001) Nonspecific adherence and fibril biogenesis by *Actinobacillus actinomycetemcomitans*: TadA protein is an ATPase. *J Bacteriol* **183:** 5927–5936.
Bhaya, D., Takahashi, A., and Grossman, A.R. (2001) Light regulation of type IV pilus-dependent motility by chemosensor-like elements in *Synechocystis* PCC6803. *Proc Natl Acad Sci USA* **98:** 7540–7545.
Boetius, A., Ravenschlag, K., Schubert, C.J., Rickert, D., Widdel, F., Gieseke, A., *et al.* (2000) A marine microbial consortium apparently mediating anaerobic oxidation of methane. *Nature* **407:** 623–626.
Brock, T.D., Brock, K.M., Belly, R.T., and Weiss, R.L. (1972) *Sulfolobus*: a new genus of sulfur-oxidizing bacteria living at low pH and high temperature. *Arch Microbiol* **84:** 54–68.
Cannio, R., Contursi, P., Rossi, M., and Bartolucci, S. (1998) An autonomously replicating transforming vector for *Sulfolobus solfataricus*. *J Bacteriol* **180:** 3237–3240.
Cohen-Krausz, S., and Trachtenberg, S. (2002) The structure of the archeabacterial flagellar filament of the extreme halophile *Halobacterium salinarum* R1M1 and its relation to eubacterial flagellar filaments and type IV pili. *J Mol Biol* **321:** 383–395.
Cohen-Krausz, S., and Trachtenberg, S. (2008) The flagellar filament structure of the extreme acidothermophile *Sulfolobus shibatae* B12 suggests that archaeabacterial flagella have a unique and common symmetry and design. *J Mol Biol* **375:** 1113–1124.
Constantinesco, F., Forterre, P., Koonin, E.V., Aravind, L., and Elie, C. (2004) A bipolar DNA helicase gene, *herA*, clusters with *rad50*, *mre11* and *nurA* genes in thermophilic archaea. *Nucleic Acids Res* **32:** 1439–1447.
Davey, M.E., and O'Toole, G.A. (2000) Microbial biofilms: from ecology to molecular genetics. *Microbiol Mol Biol Rev* **64:** 847–867.
Dorazi, R., Gotz, D., Munro, S., Bernander, R., and White, M.F. (2007) Equal rates of repair of DNA photoproducts in transcribed and non-transcribed strands in *Sulfolobus solfataricus*. *Mol Microbiol* **63:** 521–529.
Elasri, M.O., and Miller, R.V. (1999) Study of the response of a biofilm bacterial community to UV radiation. *Appl Environ Microbiol* **65:** 2025–2031.
Faguy, D.M., Jarrell, K.F., Kuzio, J., and Kalmokoff, M.L. (1994) Molecular analysis of archael flagellins: similarity to the type IV pilin-transport superfamily widespread in bacteria. *Can J Microbiol* **40:** 67–71.
Fröls, S., Gordon, P.M., Panlilio, M.A., Duggin, I.G., Bell, S.D., Sensen, C.W., and Schleper, C. (2007) Response of the hyperthermophilic archaeon *Sulfolobus solfataricus* to UV damage. *J Bacteriol* **189:** 8708–8718.
Gasson, M.J., and Davies, F.L. (1980) High-frequency conjugation associated with *Streptococcus lactis* donor cell aggregation. *J Bacteriol* **143:** 1260–1264.
Ghigo, J.M. (2001) Natural conjugative plasmids induce bacterial biofilm development. *Nature* **412:** 442–445.
Götz, D., Paytubi, S., Munro, S., Lundgren, M., Bernander, R., and White, M.F. (2007) Responses of hyperthermophilic crenarchaea to UV irradiation. *Genome Biol* **8:** R220.
van Heel, M., Schatz, M., and Orlova, E. (1992) Correlation functions revisited. *Ultramicroscopy* **46:** 307–316.
Hopfner, K.P., Putnam, C.D., and Tainer, J.A. (2002) DNA double-strand break repair from head to tail. *Curr Opin Struct Biol* **12:** 115–122.
Jonuscheit, M., Martusewitsch, E., Stedman, K.M., and Schleper, C. (2003) A reporter gene system for the hyperthermophilic archaeon *Sulfolobus solfataricus* based on a selectable and integrative shuttle vector. *Mol Microbiol* **48:** 1241–1252.
Kachlany, S.C., Planet, P.J., Bhattacharjee, M.K., Kollia, E., DeSalle, R., Fine, D.H., and Figurski, D.H. (2000) Nonspecific adherence by *Actinobacillus actinomycetemcomitans* requires genes widespread in bacteria and archaea. *J Bacteriol* **182:** 6169–6176.
Kachlany, S.C., Planet, P.J., DeSalle, R., Fine, D.H., and Figurski, D.H. (2001) Genes for tight adherence of *Actinobacillus actinomycetemcomitans*: from plaque to plague to pond scum. *Trends Microbiol* **9:** 429–437.
Kagawa, H.K., Yaoi, T., Brocchieri, L., McMillan, R.A., Alton, T., and Trent, J.D. (2003) The composition, structure and stability of a group II chaperonin are temperature regulated in a hyperthermophilic archaeon. *Mol Microbiol* **48:** 143–156.
Kawakami, Y., Ito, T., Kamekura, M., and Nakayama, M. (2005) Ca(2+)-dependent cell aggregation of halophilic archaeon, *Halobacterium salinarum*. *J Biosci Bioeng* **100:** 681–684.
Kawakami, Y., Hayashi, N., Ema, M., and Nakayama, M. (2007) Effects of divalent cations on *Halobacterium salinarum* cell aggregation. *J Biosci Bioeng* **104:** 42–46.
Klemm, P., Hjerrild, L., Gjermansen, M., and Schembri, M.A. (2004) Structure–function analysis of the self-recognizing Antigen 43 autotransporter protein from *Escherichia coli*. *Mol Microbiol* **51:** 283–296.
Köhler, R., Schafer, K., Muller, S., Vignon, G., Diederichs, K., Philippsen, A., *et al.* (2004) Structure and assembly of the pseudopilin PulG. *Mol Microbiol* **54:** 647–664.
Kosa, J.L., Zdraveski, Z.Z., Currier, S., Marinus, M.G., and Essigmann, J.M. (2004) RecN and RecG are required for *Escherichia coli* survival of Bleomycin-induced damage. *Mutat Res* **554:** 149–157.
Kuluncsics, Z., Perdiz, D., Brulay, E., Muel, B., and Sage, E. (1999) Wavelength dependence of ultraviolet-induced DNA damage distribution: involvement of direct or indirect mechanisms and possible artefacts. *J Photochem Photobiol B* **49:** 71–80.
LaPaglia, C., and Hartzell, P.L. (1997) Stress-induced production of biofilm in the hyperthermophile *Archaeoglobus fulgidus*. *Appl Environ Microbiol* **63:** 3158–3163.
Martin, A., Yeats, S., Janekovic, D., Reiter, W.D., Aicher, W., and Zillig, W. (1984) SAV 1, a temperate u.v.-inducible DNA virus-like particle from the archaebacterium *Sulfolobus acidocaldarius* isolate B12. *EMBO J* **3:** 2165–2168.

Martinez, L.R., and Casadevall, A. (2007) *Cryptococcus neoformans* biofilm formation depends on surface support and carbon source and reduces fungal cell susceptibility to heat, cold, and UV light. *Appl Environ Microbiol* **73:** 4592–4601.

Martusewitsch, E., Sensen, C.W., and Schleper, C. (2000) High spontaneous mutation rate in the hyperthermophilic archaeon *Sulfolobus solfataricus* is mediated by transposable elements. *J Bacteriol* **182:** 2574–2581.

Mattick, J.S. (2002) Type IV pili and twitching motility. *Annu Rev Microbiol* **56:** 289–314.

Mayerhofer, L.E., Macario, A.J., and de Macario, E.C. (1992) Lamina, a novel multicellular form of *Methanosarcina mazei* S-6. *J Bacteriol* **174:** 309–314.

Moissl, C., Rudolph, C., Rachel, R., Koch, M., and Huber, R. (2003) *In situ* growth of the novel SM1 euryarchaeon from a string-of-pearls-like microbial community in its cold biotope, its physical separation and insights into its structure and physiology. *Arch Microbiol* **180:** 211–217.

Moissl, C., Rachel, R., Briegel, A., Engelhardt, H., and Huber, R. (2005) The unique structure of archaeal 'hami', highly complex cell appendages with nano-grappling hooks. *Mol Microbiol* **56:** 361–370.

Molin, S., and Tolker-Nielsen, T. (2003) Gene transfer occurs with enhanced efficiency in biofilms and induces enhanced stabilisation of the biofilm structure. *Curr Opin Biotechnol* **14:** 255–261.

Näther, D.J., Rachel, R., Wanner, G., and Wirth, R. (2006) Flagella of *Pyrococcus furiosus*: multifunctional organelles, made for swimming, adhesion to various surfaces, and cell–cell contacts. *J Bacteriol* **188:** 6915–6923.

Nutsch, T., Marwan, W., Oesterhelt, D., and Gilles, E.D. (2003) Signal processing and flagellar motor switching during phototaxis of *Halobacterium salinarum*. *Genome Res* **13:** 2406–2412.

O'Toole, G.A., and Kolter, R. (1998) Flagellar and twitching motility are necessary for *Pseudomonas aeruginosa* biofilm development. *Mol Microbiol* **30:** 295–304.

O'Toole, G.A., Gibbs, K.A., Hager, P.W., Phibbs, P.V., Jr, and Kolter, R. (2000) The global carbon metabolism regulator Crc is a component of a signal transduction pathway required for biofilm development by *Pseudomonas aeruginosa*. *J Bacteriol* **182:** 425–431.

Ojanen-Reuhs, T., Kalkkinen, N., Westerlund-Wikstrom, B., van Doorn, J., Haahtela, K., Nurmiaho-Lassila, E.L., *et al.* (1997) Characterization of the *fimA* gene encoding bundle-forming fimbriae of the plant pathogen *Xanthomonas campestris* pv. *vesicatoria*. *J Bacteriol* **179:** 1280–1290.

Oostergetel, G.T., Keegstra, W., and Brisson, A. (1998) Automation of specimen selection and data acquisition for protein electron crystallography. *Ultramicroscopy* **74:** 47–59.

Patel, R. (2005) Biofilms and antimicrobial resistance. *Clin Orthop Relat Res* **437:** 41–47.

Peabody, C.R., Chung, Y.J., Yen, M.R., Vidal-Ingigliardi, D., Pugsley, A.P., and Saier, M.H., Jr (2003) Type II protein secretion and its relationship to bacterial type IV pili and archaeal flagella. *Microbiology* **149:** 3051–3072.

Penczek, P., Radermacher, M., and Frank, J. (1992) Three-dimensional reconstruction of single particles embedded in ice. *Ultramicroscopy* **40:** 33–53.

Planet, P.J., Kachlany, S.C., DeSalle, R., and Figurski, D.H. (2001) Phylogeny of genes for secretion NTPases: identification of the widespread tadA subfamily and development of a diagnostic key for gene classification. *Proc Natl Acad Sci USA* **98:** 2503–2508.

Reilly, M.S., and Grogan, D.W. (2002) Biological effects of DNA damage in the hyperthermophilic archaeon *Sulfolobus acidocaldarius*. *FEMS Microbiol Lett* **208:** 29–34.

Reisner, A., Holler, B.M., Molin, S., and Zechner, E.L. (2006) Synergistic effects in mixed *Escherichia coli* biofilms: conjugative plasmid transfer drives biofilm expansion. *J Bacteriol* **188:** 3582–3588.

Roine, E., Raineri, D.M., Romantschuk, M., Wilson, M., and Nunn, D.N. (1998) Characterization of type IV pilus genes in *Pseudomonas syringae* pv. *tomato* DC3000. *Mol Plant Microbe Interact* **11:** 1048–1056.

Rosenshine, I., Tchelet, R., and Mevarech, M. (1989) The mechanism of DNA transfer in the mating system of an archaebacterium. *Science* **245:** 1387–1389.

Sauvonnet, N., Vignon, G., Pugsley, A.P., and Gounon, P. (2000) Pilus formation and protein secretion by the same machinery in *Escherichia coli*. *EMBO J* **19:** 2221–2228.

Schelert, J., Dixit, V., Hoang, V., Simbahan, J., Drozda, M., and Blum, P. (2004) Occurrence and characterization of mercury resistance in the hyperthermophilic archaeon *Sulfolobus solfataricus* by use of gene disruption. *J Bacteriol* **186:** 427–437.

Schleper, C., Roder, R., Singer, T., and Zillig, W. (1994) An insertion element of the extremely thermophilic archaeon *Sulfolobus solfataricus* transposes into the endogenous beta-galactosidase gene. *Mol Gen Genet* **243:** 91–96.

Schleper, C., Holz, I., Janekovic, D., Murphy, J., and Zillig, W. (1995) A multicopy plasmid of the extremely thermophilic archaeon *Sulfolobus* effects its transfer to recipients by mating. *J Bacteriol* **177:** 4417–4426.

Schopf, S., Wanner, G., Rachel, R., and Wirth, R. (2008) An archaeal bi-species biofilm formed by *Pyrococcus furiosus* and *Methanopyrus kandleri*. *Arch Microbiol* **190:** 371–377.

Shapiro, J.A. (1998) Thinking about bacterial populations as multicellular organisms. *Annu Rev Microbiol* **52:** 81–104.

Szabó, Z., Albers, S.V., and Driessen, A.J.M. (2006) Active-site residues in the type IV prepilin peptidase homologue PibD from the archaeon *Sulfolobus solfataricus*. *J Bacteriol* **188:** 1437–1443.

Szabó, Z., Sani, M., Groeneveld, M., Zolghadr, B., Schelert, J., Albers, S.V., *et al.* (2007a) Flagellar motility and structure in the hyperthermoacidophilic archaeon *Sulfolobus solfataricus*. *J Bacteriol* **189:** 4305–4309.

Szabó, Z., Stahl, A.O., Albers, S.V., Kissinger, J.C., Driessen, A.J.M., and Pohlschroder, M. (2007b) Identification of diverse archaeal proteins with class III signal peptides cleaved by distinct archaeal prepilin peptidases. *J Bacteriol* **189:** 772–778.

Wang, Y.A., Yu, X., Ng, S.Y., Jarrell, K.F., and Egelman, E.H. (2008) The structure of an archaeal pilus. *J Mol Biol* **381:** 456–466.

Wood, E.R., Ghane, F., and Grogan, D.W. (1997) Genetic responses of the thermophilic archaeon *Sulfolobus acidocaldarius* to short-wavelength UV light. *J Bacteriol* **179:** 5693–5698.

Zolghadr, B., Weber, S., Szabó, Z., Driessen, A.J.M., and Albers, S.V. (2007) Identification of a system required for the functional surface localization of sugar binding proteins with class III signal peptides in *Sulfolobus solfataricus*. *Mol Microbiol* **64:** 795–806.

Supporting information

Additional supporting information may be found in the online version of this article.

Please note: Wiley-Blackwell are not responsible for the content or functionality of any supporting materials supplied by the authors. Any queries (other than missing material) should be directed to the corresponding author for the article.

UV-inducible cellular aggregation of the hyperthermophilic archaeon *Sulfolobus solfataricus* is mediated by pili formation

Sabrina Fröls[1,2], Magorzata Ajon [3], Michaela Wagner[3], Daniela Teichmann[1], Behnam Zolghadr [3] , Mihaela Folea[4], Egbert J. Boekema[4], Arnold J.M. Driessen[3], Christa Schleper[1,2#] and Sonja-Verena Albers[3]

[1] Department of Genetics in Ecology, Vienna Ecology Center, University of Vienna, Althanstrasse 14, 1090 Vienna, Austria

[2] Center for Geobiology, Department of Biology, University of Bergen, Realfagbygget, Allegaten 41, N-5007 Bergen

[3] Department of Microbiology, Groningen Biomolecular Sciences and Biotechnology Institute and the Zernike Institute for Advanced Materials, University of Groningen, Kerklaan 30, 9751 NN Haren, The Netherlands

[4]Department of Biophysical Chemistry, Groningen Biomolecular Sciences and Biotechnology Institute, University of Groningen, Nijenborgh 4, 9747 AG Groningen, The Netherlands

[#]Correspondence to C. Schleper, e-mail: christa.schleper@univie.ac.at,
tel: +43 14277 57800, fax: +43 14277 9578

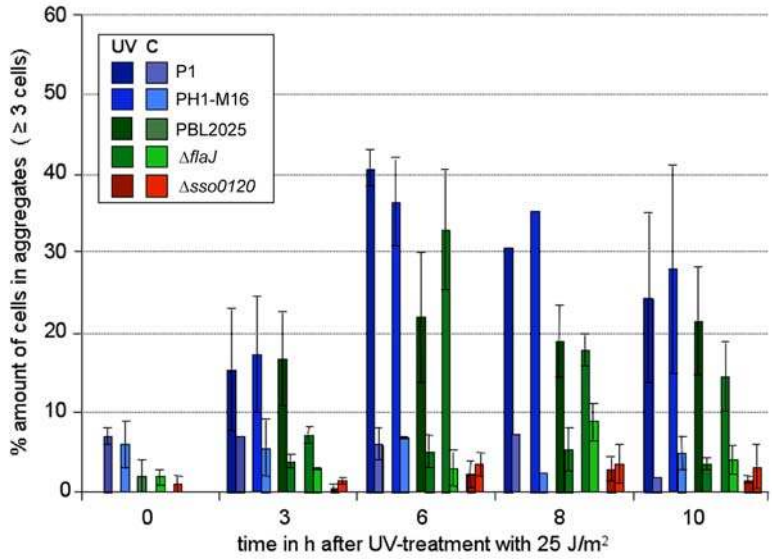

Fig. S1: Quantitative analysis of the UV-induced cellular aggregation of different *S. solfataricus* strains. Cellular aggregation was observed at 3, 6, 8, and 10 hours after UV-treatment with 25 J/m^2 (254 nm). The graph is based on three independent UV-experiments; in the case of the strains PBL2025, Δ*flaJ* and Δ*sso0120* and 2 independent UV-experiments for the strains P1 and PH1-M16 (only one experiment at 8 h, respectively). The bars display the % amount of cells in aggregates (≥ 3 cells) in relation to the total amount of evaluated cells (at minimum 500 single cells were counted, but mostly up to 1000).

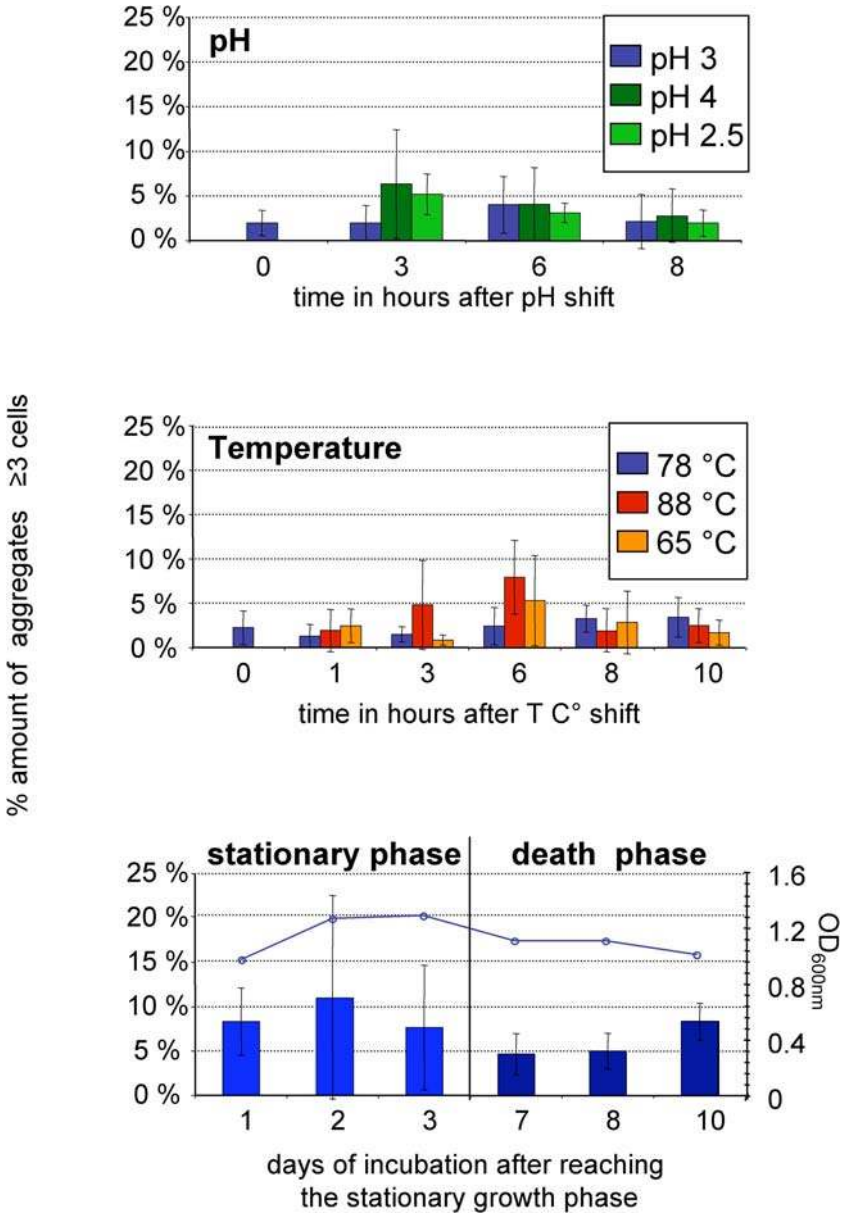

Fig. S2: Quantitative analysis of the cellular aggregation under different environmental stressors and cell growth: non-lethal pH shift, from pH 3 to pH 4 and down to pH 2.5 and a non-lethal temperature shift from 78°C up to 88°C and down to 65°C, early stationary growth phase until dead phase. The bars represent the mean of the results obtained for the four *sso0120* wild type strains; P1, PH1-M16, PBL2025 and Δ*flaJ*. The % amount of cells in aggregates (≥ 3 cells) in relation to the total amount of evaluated cells (500 single cells, or a minimum of 250 single cells were counted).

Table S1 : *Primers used in this study*

Primer name	Sequenz (5'-3')
1 RT forward	ATAGGTCAAGTGATGGGTTA
1 RT reverse	CATCTGCTGCAAGTATCTTT
2 RT forward	GCCTATACGCATGGTTTCAC
2 RT reverse	AAGGGTCAGCTAAGGGTACA
3 RT forward	AGCAAGAAGATCACGTACTA
3 RT reverse	CTGGAGTATCCTCTATGGTAAT
4 RT forward	GATCTAGAAGAGTTCAGTGTT
4 RT reverse	AGACCTTGGCTCTGCTTTCC
5 RT forward	ACACAAGTGGTGAGTCAATA
5 RT reverse	TTTGCAGCGAGTTCTCCTAA
6 RT forward	AGGGCAGTTGGCAACTTAGA
6 RT reverse	ATATCTGTGTGCTGCCGGTA
7 RT forward	GCTGGGTGGTCTACTTTATG
7 RT reverse	AGTACTGCCCAGCAGTTA
118 forward-*Nco*I	CCCCCCCATGGTACAACTAATGATGAAAGGAGG*
118 reverse-*Bam*HI	CCCCCGGATCCCGCTATTGAAGCCAGCA
117 reverse-*Bam*HI	CCCCCGGATCCATCCGGTCCAGAGTTGA
121 forward-*Nco*I	CCCCCCATGGCAATTCCAGATTTTATACTATATCAG
KO-UP forward	CCCGGTACCGTGCGTATTATCTACGTTA
KO-UP reverse	CCCCCATGGCAGTGTTTATTTAAAGAA
KO-DOWN forward	CCCGGATCCGGAGAATATTCATGATAC
KO-DOWN reverse	CCCCCCCCCGCGGCCGCCGAGTGCAAAGATACTTG

* restriction sites are underlined

Table S2: *Homologous ups-operons in other Archaea*

S. solfataricus	Length in aa	*S. tokodaii*	*S. acidocaldarius*	*Metalosphera sedula*
SSO0121	695	ST1396	Saci_1493	Msed_2103
SSO0120	483	ST1397	Saci_1494	Msed_2104
SSO0119	481	ST1398	Saci_1495	Msed_2105
SSO0118	154	ST1399	Saci_1496	Msed_1193
SSO0117	137	ST1400	Saci_1496a*	Msed_2107

* not annotated, found by tblastn search on position 1275628-1275993 in the genome of *S. acidocaldarius* (amino acid identity 30 %, similarity 60 %)